

Heavy-Quark Expansion for $\bar{B}_s \rightarrow D_s^{(*)}$ Form Factors and Unitarity Bounds beyond the $SU(3)_F$ Limit

Marzia Bordone*

Universität Siegen, Walter-Flex Straße 3, 57072 Siegen, Germany

Nico Gubernari† and Danny van Dyk‡

Technische Universität München, James-Frank-Straße 1, 85748 Garching, Germany

Martin Jung§

Dipartimento di Fisica, Università di Torino & INFN, Sezione di Torino, I-10125 Torino, Italy

We carry out a comprehensive analysis of the full set of $\bar{B}_q \rightarrow D_q^{(*)}$ form factors for spectator quarks $q = u, d, s$ within the framework of the Heavy-Quark Expansion (HQE) to order $\mathcal{O}(\alpha_s, 1/m_b, 1/m_c^2)$. In addition to the available lattice QCD calculations we make use of two new sets of theoretical constraints: we produce for the first time numerical predictions for the full set of $\bar{B}_s \rightarrow D_s^{(*)}$ form factors using Light-Cone Sum Rules with B_s -meson distribution amplitudes. Furthermore, we reassess the QCD three-point sum rule results for the Isgur-Wise functions entering all our form factors for both $q = u, d$ and $q = s$ spectator quarks. These additional constraints allow us to go beyond the commonly used assumption of $SU(3)_F$ symmetry for the $\bar{B}_s \rightarrow D_s^{(*)}$ form factors, especially in the unitarity constraints which we impose throughout our analysis. We find the coefficients of the IW functions emerging at $\mathcal{O}(1/m_c^2)$ to be consistent with the naive $\mathcal{O}(1)$ expectation, indicating a good convergence of the HQE. While we do not find significant $SU(3)$ breaking, the explicit treatment of $q = s$ as compared to a simple symmetry assumption renders the unitarity constraints more effective. We find that the (pseudo)scalar bounds are saturated to a large degree, which affects our theory predictions. We analyze the phenomenological consequences of our improved form factors by extracting $|V_{cb}|$ from $\bar{B} \rightarrow D^{(*)}\ell\nu$ decays and producing theoretical predictions for the lepton-flavour universality ratios $R(D)$, $R(D^*)$, $R(D_s)$ and $R(D_s^*)$, as well as the τ - and D_q^* polarization fractions for the $\bar{B}_q \rightarrow D_q^{(*)}\tau\nu$ modes.

I. INTRODUCTION

Semileptonic $b \rightarrow c$ transitions are of great phenomenological interest, both within the Standard Model (SM) and beyond. The foreseeable improved precision for the corresponding measurements [1–3] requires a corresponding improvement in their theoretical description. Additional interest is created by the long-standing tensions in semitauonic decays and neutral-current $b \rightarrow s\ell^+\ell^-$ transitions, as well as the difference between inclusive and exclusive determinations of the CKM matrix element $|V_{cb}|$ [4]. These tensions motivate potential new physics (NP) contributions to $b \rightarrow c\ell\nu$ transitions with light leptons, which in turn require a determination of the corresponding form factors independent of the experimental input. This situation, together with the recent appearance of several experimental analysis allowing for a model-independent interpretation of their results on $\bar{B} \rightarrow D^{(*)}\ell\nu$ decays [5–7] sparked renewed interest in the relevant hadronic matrix elements [8–18]. A recent theory analysis of the form factors parametrizing the $\bar{B} \rightarrow D^{(*)}$ matrix element by three of us [19] uses the heavy-quark expansion to determine the full set of relevant parameters up to order $1/m_c^2$ for the first time, building and improving on the work presented in refs. [8, 15, 20] in particular. This analysis also uses unitarity bounds to restrict the parameter space of the so-called Isgur-Wise (IW) functions [21, 22]. Specifically, it was observed that for $J^P = 0^+$ and 0^- currents the present results saturate the bounds to a large degree. This observation triggers our interest, since $SU(3)_F$ symmetry breaking at the level of 20% is assumed for the form factors in these bounds, with the effect of *lowering* the values of the form factors and therefore lowering the contributions to the unitarity bounds by 40%. For a precision analysis of the form factors this assumption should be removed, and instead a simultaneous analysis of the form factors for both light ($q = u, d$) and strange ($q = s$) spectator quarks is warranted. The purpose of this article is to carry out such a simultaneous analysis. For this work we take the following steps:

* marzia.bordone@uni-siegen.de

† nicogubernari@gmail.com

‡ danny.van.dyk@gmail.com

§ martin.jung@unito.it

- We estimate the normalization and the slope of the subleading IW functions η , χ_2 , and χ_3 , as well as $\eta^{(s)}$, $\chi_2^{(s)}$, and $\chi_3^{(s)}$ in the point of zero hadronic recoil, based on existing analytical formulas in the literature [23–25]. The necessary numerical inputs and our numerical results are compiled in appendix A.
- We estimate the full set of $\bar{B}_s \rightarrow D_s^{(*)}$ form factors needed for the basis of dimension-six effective operators $b \rightarrow c\ell\nu$ using light-cone sum rules with B -meson LCDAs. The relevant analytical results have been recently published in ref. [26], and their numerical implementation as part of the EOS software [27] facilitates this step. The necessary numerical inputs and our numerical results including correlation information are compiled in appendix B. Our numerical results for the $\bar{B}_s \rightarrow D_s^*$ transitions allow to carry out our analysis at the complete $\mathcal{O}(1/m_c^2)$ level.
- With the theoretical constraints at hand, we simultaneously infer the parameters of the various form factors within the HQE, in three different fit models. In all of our analyses, we impose the strong unitarity bounds for all $\bar{B}_q^{(*)} \rightarrow D_q^{(*)}$ transitions.

Note that some of the results from ref. [19] are superseded by our new results.

The structure of this article is as follows. We briefly introduce the necessary notation and set up our analysis in section II. We discuss the results in section III, and summarize in section IV. In appendix A we provide the numerical inputs and results of the updated QCDSR analysis. In appendix B we provide the numerical inputs and results of our LCSR analysis.

II. NOTATION AND SETUP

We analyse the full set of hadronic matrix elements for the basis of local dimension-three currents $\bar{c}\Gamma b$ in $\bar{B}_q \rightarrow D_q^{(*)}$ transitions. For this purpose, we use the heavy-quark expansion (HQE) as reviewed in ref. [8], and as applied recently in refs. [15, 19]. Within the expansion of a generic form factor $h(w)$,

$$h(w) = \xi(w)\hat{h}(w) = \xi(w) \left(a + \hat{\alpha}_s b + \varepsilon_b c_b^{(i)} \left[\hat{L}_i(w) \right] + \varepsilon_c c_c^{(i)} \left[\hat{L}_i(w) \right] + \varepsilon_c^2 d^{(i)} \left[\hat{\ell}_i(w) \right] \right) \quad (1)$$

one encounters three expansion parameters: $\hat{\alpha}_s \equiv \alpha_s/\pi$, $\varepsilon_b \equiv \bar{\Lambda}/(2m_b)$, and $\varepsilon_c \equiv \bar{\Lambda}/(2m_c)$. The coefficients a , b , $c_b^{(i)}$, $c_c^{(i)}$, and $d^{(i)}$ in this expansion are linear combinations of Wilson coefficients from the matching of HQET onto QCD and kinematic functions. The objects $\xi(w)$, $L_i(w)$, and $\ell_i(w)$ are matrix elements of the effective operator in HQET, the IW functions. To differentiate between matrix elements with a light or a strange spectator quark, we will add the label “(s)” where appropriate. This includes the IW functions entering $\bar{B}_s^{(*)} \rightarrow D_s^{(*)}$, as well as $\bar{\Lambda}_{(s)}$, the energy of the light degrees of freedom within the heavy meson in the heavy-quark limit. For the analysis at hand we use the same power counting of the HQE as introduced in ref. [19] (i.e., $\hat{\alpha}_s \sim \varepsilon_b \sim \varepsilon_c^2 \sim \varepsilon^2$). We also use the same nominal fit model, *i.e.*, the 3/2/1 model, where the digits refer to the power in the z expansion to which the IW functions are expanded at different orders in $1/m_q$. In case of the 3/2/1 model we use z^3 for the leading IW function, z^2 for subleading IW functions, and z^1 for the subsubleading IW functions.

A key point of our analysis is the treatment of the $SU(3)_F$ symmetry breaking in all IW functions. For a large part of the analysis we do not make any assumption about the size of this breaking, but simply parametrize the $q = s$ IW functions with independent parameters. Only in one of our scenarios, to be discussed below, we assume that the subsubleading IW functions behave schematically as

$$\ell_i^{(s)}(w) = \ell_i(w) + \varepsilon_F \delta_{\ell_i}(w), \quad (2)$$

with $\varepsilon_F \sim \varepsilon_c$ (and $\delta_{\ell_i} \sim \ell_i$). This assumption is subsequently confronted with the available data.

In addition to the theoretical constraints for the $\bar{B} \rightarrow D^{(*)}$ form factors with spectators $q = u, d$ as used in ref. [19], we include further theory information on the form factors with $q = s$ spectators. The individual *changed or new* pieces of theory information entering the likelihood are:

Lattice: For $\bar{B}_s \rightarrow D_s$ the HPQCD collaboration [28] has determined both the vector form factor $f_+^{(s)}$ and the scalar form factor $f_0^{(s)}$ at non-zero hadronic recoil $w \geq 1$. Accounting for the fact that at $w = w_{\max,D}$ the two form factors fulfill an equation of motion, we can produce 5 correlated pseudo data points from the correlated parameters provided in ref. [28]. In addition, lattice QCD data by the ETM collaboration has been used in ref. [29] to determine $f_+^{(s)}$ and the ratios $f_T^{(s)}/f_+^{(s)}$ and $f_0^{(s)}/f_+^{(s)}$ close to the zero recoil point at $q^2 = 11.5 \text{ GeV}^2$.

We do not use the the result for $f_+^{(s)}$ nor for the ratio $f_0^{(s)}/f_+^{(s)}$ due to their large uncertainties, which are not competitive with the HPQCD result. We do use, however, the ratio $f_T^{(s)}/f_+^{(s)}$, thereby including one further data point in the fit.

In addition to the $q = s$ constraints, ref. [29] also provides results for $\bar{B} \rightarrow D$ form factors, which did not enter the previous analysis. Following the same argument as before, we only use the constraint on f_T/f_+ , thereby including one further data point.

For theory predictions of observables in nonleptonic $\bar{B} \rightarrow D\pi$ decays in the context of QCD factorization, the FNAL/MILC collaborations have calculated, amongst other quantities, the ratio $f_0^{(s)}(q^2 = M_\pi^2)/f_0(q^2 = M_\pi^2)$ [30]. The results of ref. [30] for $q = u, d$ form factors are superseded by those of ref. [31], which feature much smaller statistical uncertainties. This is due to the use of a larger number of gauge ensembles (14 vs 4), which in turn reduces the statistical correlation between the results of refs. [30] and [31]. We use this $q = s$ vs $q = u, d$ ratio as part of our fit whenever both $q = u, d$ and $q = s$ information is included.

For $\bar{B}_s \rightarrow D_s^*$ the HPQCD collaboration has determined the form factor $h_{A_1}^{(s)}$ at zero recoil or equivalently $w = 1$ [32], which is used in all fits.

QCDSR: The QCD three-point sum rules used to estimate the normalization and slopes for the subleading-power IW functions at $w = 1$ and for $q = u, d$ can be adapted for the $q = s$ case. In order to ensure a consistent treatment of both parametric and systematic uncertainties, we update the $q = u, d$ analysis and carry out a new $q = s$ analysis. The relevant inputs, the procedure to determine the uncertainties, and our numerical results are discussed in appendix A.

LCSR: At $w \geq 1.5$ the $\bar{B}_s \rightarrow D_s^{(*)}$ form factor are accessible in LCSRs with B_s -meson Light-Cone Distribution Amplitudes (LCDAs). Following the recent analytic results for the light-cone OPE of the correlation functions underlying these sum rules in ref. [26], we produce the first numerical estimates of the $\bar{B}_s \rightarrow D_s^{(*)}$ form factors in this approach. Our numerical results for the $\bar{B}_s \rightarrow D_s^*$ form factors, including their correlations, are provided as machine-readable ancillary files with the arXiv preprint version of this paper. As in ref. [26], we are unable to produce reliable results for the $\bar{B}_s \rightarrow D_s$ form factor f_T , which is therefore not used in our analysis. The new constraints contribute a total of 33 data points to all fits. The relevant inputs and the procedure to determine the uncertainties are discussed in appendix B.

For the fits to the available theory constraints we consider the following scenarios:

- A:** We fit to only $\bar{B}_s \rightarrow D_s^{(*)}$ information in the 3/2/1 model. In order to use the unitarity bounds, we multiply the contributions to the bound by a factor $n_s = 2.2$. This factor accounts for the strange-spectator contributions, and uses $SU(3)_F$ -symmetry to approximate the $q = u, d$ spectator contributions. In this way, we allow for symmetry breaking of -20% on the amplitude level. This scenario encompasses 23 parameters.
- B:** We fit simultaneously to $\bar{B}_{u,d,s} \rightarrow D_{u,d,s}^{(*)}$ information in the 3/2/1 model. We treat all IW functions for the light and the strange spectator quarks as fully independent. In this way, we introduce the least possible amount of correlation between the form factors, which only arises from the contributions to the strong unitarity bounds. As a consequence, our fit has twice the number of free parameters as in the fit in ref. [19], corresponding to 46 parameters.
- C:** As scenario B, but additionally we consider the impact of finite $SU(3)_F$ symmetry breaking in the form factors by amending our previous power counting: we count the expansion parameter ε_F for the symmetry breaking as $\varepsilon_F \sim \varepsilon \sim \varepsilon_c$. With this power-counting, a generic form factor $h^{(s)}$ receives contributions from the subsubleading IW functions that can be expressed schematically as:

$$\begin{aligned} h^{(s)}(w) &\supseteq \varepsilon_c^2 \ell_i^{(s)}(w) = \varepsilon_c^2 \ell_i(w) + \varepsilon_c^2 \varepsilon_F \delta_{\ell_i}(w) \\ &\sim \varepsilon^2 \ell_i(w) + \varepsilon^3 \delta_{\ell_i}(w). \end{aligned} \tag{3}$$

Since we discard terms at order ε^3 , we suppress the symmetry-breaking terms δ_{ℓ_i} of the subsubleading IW functions and identify $\ell_i^{(s)}(w) = \ell_i(w)$ *in this scenario only*. In this way, we reduce the number of free parameters to 34.

likelihood	#data pts	#par	A	B	C	C
			23	46	34	34
lattice(D_s)	6		0.26	0.49	1.10	1.25
lattice(D_s^*)	1		0.00	0.00	0.47	0.45
QCDSR $\bar{B}_s \rightarrow D_s^{(*)}$	5		0.15	0.11	0.29	0.23
LCSR $\bar{B}_s \rightarrow D_s^{(*)}$	33		1.26	1.11	1.43	1.58
lattice(D)	(13)		—	7.16	8.02	8.19
lattice(D^*)	(1)		—	0.01	0.59	0.61
QCDSR $\bar{B} \rightarrow D^{(*)}$	(5)		—	0.08	0.24	0.25
LCSR $\bar{B} \rightarrow D^{(*)}$	(33)		—	3.11	2.86	2.78
lattice ratio (D_s/D)	(1)		—	0.58	0.77	1.00
$\bar{B} \rightarrow D\{e^-, \mu^-\}\bar{\nu}$	(9)		—	—	—	6.87
$\bar{B} \rightarrow D^*\{e^-, \mu^-\}\bar{\nu}$ 2017	(9)		—	—	—	7.73
$\bar{B} \rightarrow D^*\{e^-, \mu^-\}\bar{\nu}$ 2018	(9)		—	—	—	5.34
	45		1.68	—	—	—
total	(98)		—	12.67	15.75	—
	(125)		—	—	—	36.27

TABLE I. Summary of the goodness of fit in terms of the χ^2 values at the best-fit point for all combinations of fit scenarios and datasets.

III. RESULTS

In the following we describe the fits that are part of our analysis, in terms of the combination of likelihoods and parameter scenarios, focusing in particular on the impact of the improved unitarity constraints and quantifying the amount of $SU(3)_F$ breaking. A summary of their goodness of fit, expressed through the χ^2 values at the best-fit point, is given in table I.

We begin with fitting the restricted theory likelihood, which includes exclusively the 45 $q = s$ data points. For this likelihood, only fit scenario A with its 23 parameters is applicable. We obtain a very good fit with a minimal $\chi^2/\text{d.o.f.} \sim 2/22$. The very small χ^2 value is not very surprising, given the large systematic uncertainties assigned to the QCDSR and LCSR data points. A first step to test the assumption of exact $SU(3)_F$ symmetry is taken by evaluating our nominal likelihood at the best-fit point obtained in ref. [19] from the combination of the theoretical and experimental likelihoods. We find excellent compatibility of the total likelihood, with an increase of χ^2 at the $q = u, d$ best-fit point by approximately 15. Inspecting the individual constraints, we find the largest single increase of ~ 11 is caused by the very precise lattice constraints on the $\bar{B}_s \rightarrow D_s$ form factors by the HPQCD collaboration. Nevertheless, even this shift still indicates reasonable compatibility of the lattice QCD constraint with the central value from ref. [19], with an individual p value of $\sim 10\%$. The remaining constraints are perfectly compatible with the assumption of exact $SU(3)_F$ symmetry in this simple comparison.

We continue with fitting the nominal theory likelihood, which includes all $q = u, d$ and $q = s$ data points as well as the single $q = s/q = u, d$ lattice ratio. For this likelihood, only scenarios B and C are applicable with their 46 and 34 parameters, respectively. For scenario B we find an excellent fit with $\chi^2/\text{d.o.f.} \sim 13/52$. Relative to this result, scenario C increases the d.o.f. by 12 while only increasing the χ^2 by ~ 3 . For both scenarios, the best-fit values of $q = u, d$ parameters are contained within the 68% probability intervals obtained in ref. [19]. We continue with a model comparison between the fits to the nominal likelihood in scenarios B and C. Using posterior samples we compute the model evidence for both scenarios, and hence their Bayes factor:

$$\log_{10} \frac{P(\text{nominal likelihood} \mid \text{scenario B})}{P(\text{nominal likelihood} \mid \text{scenario C})} = \log_{10} \frac{9.80 \cdot 10^{48}}{2.71 \cdot 10^{57}} \sim -8. \quad (4)$$

Using Jeffrey's scale for the interpretation of the Bayes factor [33], this result indicates that the nominal likelihood favours scenario C over scenario B *decisively*, leading to the conclusion that scenario C is — on average — much more efficient than scenario B in describing the data. Hence, we will not use scenario B from this point on.

order	function f	$f(1)$	$f'(1)$	$f''(1)$	$f'''(1)$	
$1/m_Q^0$	ξ	+1.00	—	-1.15 [-1.30, -0.98]	+2.02 [+1.64, +2.43]	-3.90 [-4.90, -3.04]
	$\xi^{(s)}$	+1.00	—	-1.13 [-1.38, -0.86]	+2.01 [+1.46, +2.68]	-3.97 [-5.54, -2.64]
$1/m_Q^1$	$\hat{\chi}_2$	-0.07 [-0.10, -0.03]	-0.02 [-0.05, +0.02]	-0.01 [-0.16, +0.18]	—	—
	$\hat{\chi}_3$	+0.00	—	+0.04 [+0.01, +0.07]	-0.11 [-0.17, -0.06]	—
	$\hat{\eta}$	+0.64 [+0.50, +0.79]	+0.06 [-0.16, +0.27]	-0.52 [-1.08, +0.01]	—	—
	$\hat{\chi}_2^{(s)}$	-0.07 [-0.10, -0.03]	-0.00 [-0.03, +0.04]	+0.15 [-0.22, +0.57]	—	—
	$\hat{\chi}_3^{(s)}$	+0.00	—	+0.03 [+0.01, +0.07]	-0.13 [-0.23, -0.03]	—
	$\hat{\eta}^{(s)}$	+0.68 [+0.53, +0.83]	-0.12 [-0.37, +0.15]	-0.73 [-1.75, +0.25]	—	—
$1/m_Q^2$	$\hat{\ell}_1$	+0.17 [-0.02, +0.37]	-5.80 [-11.6, -0.59]	—	—	—
	$\hat{\ell}_2$	-1.60 [-1.82, -1.37]	-3.73 [-8.43, +0.76]	—	—	—
	$\hat{\ell}_3$	-3.52 [-9.41, +2.49]	+5.12 [-0.04, +10.4]	—	—	—
	$\hat{\ell}_4$	-2.33 [-3.54, -1.14]	-0.72 [-2.55, +1.05]	—	—	—
	$\hat{\ell}_5$	+3.04 [+1.00, +5.10]	+0.18 [-2.01, +2.46]	—	—	—
	$\hat{\ell}_6$	+2.33 [-0.64, +5.40]	+0.70 [-2.45, +3.96]	—	—	—

TABLE II. Best-fit point for the parameters of scenario C in a simultaneous fit to theory constraints and all available experimental measurements. Uncertainty ranges presented here are meant for illustrative purpose only, and should not be interpreted as standard deviations due to non-Gaussianity of the joint posterior.

We furthermore tested the compatibility of the theory data with exact $SU(3)_F$ symmetry for *all* parameters in the IW functions. This fit shows a further increase of χ^2 by ~ 3.5 , to be compared to an increase of the d.o.f. by 11. The data therefore show no indication of $SU(3)_F$ breaking at the present level of precision. We nevertheless refrain from using this limit beyond the subsubleading IW functions, in order to allow for the possibility of a sizable breaking and to include the resulting uncertainty for the form factors and observables.

We finally fit the combined likelihood comprised of the nominal theory likelihood and the experimental likelihood containing the Belle results of the kinematical PDFs in the recoil variable w . Following the model comparison above, we only fit this likelihood with scenario C. The $\chi^2/\text{d.o.f.} \sim 36/91$ indicates an excellent fit, with an increase of χ^2 by ~ 20 for 27 additional d.o.f. Compared to the fits of the nominal theory likelihood in scenario C, the increase in the minimal χ^2 can be attributed in full to the experimental likelihood, indicating that either likelihood is well described by scenario C. We provide the best-fit point as well as the individual one-dimensional 68% probability intervals for each fit parameters in table II.

Form factor predictions With the posterior samples obtained from the fit to the nominal theory likelihood in scenario C, we produce posterior predictive distributions for all $\bar{B} \rightarrow D^{(*)}$ form factors. In figure 1, the median curves and envelopes at 68% probability are juxtaposed with those obtained using the 3/2/1 model results in ref. [19]. We find very good agreement between the respective predictions, and obtain slightly smaller uncertainties than in ref. [19]. The largest change appears in the form factor A_0 close to zero recoil, with scenario C preferring slightly larger values for this form factor than the previous analysis. The main reason for this is a strong saturation of the unitarity bound in the 0^- channel due to our removing of the implicit assumption of 20% $SU(3)_F$ breaking at the amplitude level.

We use the posterior samples from scenario A and scenario C to produce posterior predictive distributions for all $\bar{B}_s \rightarrow D_s^{(*)}$ form factors. Their respective median curves and 68% probability envelopes are juxtaposed in figure 2. The fit using scenario C significantly reduces the uncertainty of the $\bar{B}_s \rightarrow D_s^{(*)}$ form factors when compared to scenario A. This is an expected result, since in scenario C the subsubleading IW are shared between $q = u, d$ and $q = s$ spectators, and the $SU(3)_F$ breaking is taken into account explicitly in the unitarity bounds instead of weakening them by a rough estimate for the breaking.

BGL coefficients The type of form factor parametrization put forward in ref. [38] allows for a straight-forward application of the unitarity constraints and allows to put a strict upper limit on higher-order contributions. We produce posterior predictive distributions for the coefficients of this parametrization, and find their joint distribution to be accurately represented by a multivariate Gaussian distribution. Within ancillary files attached to this preprint

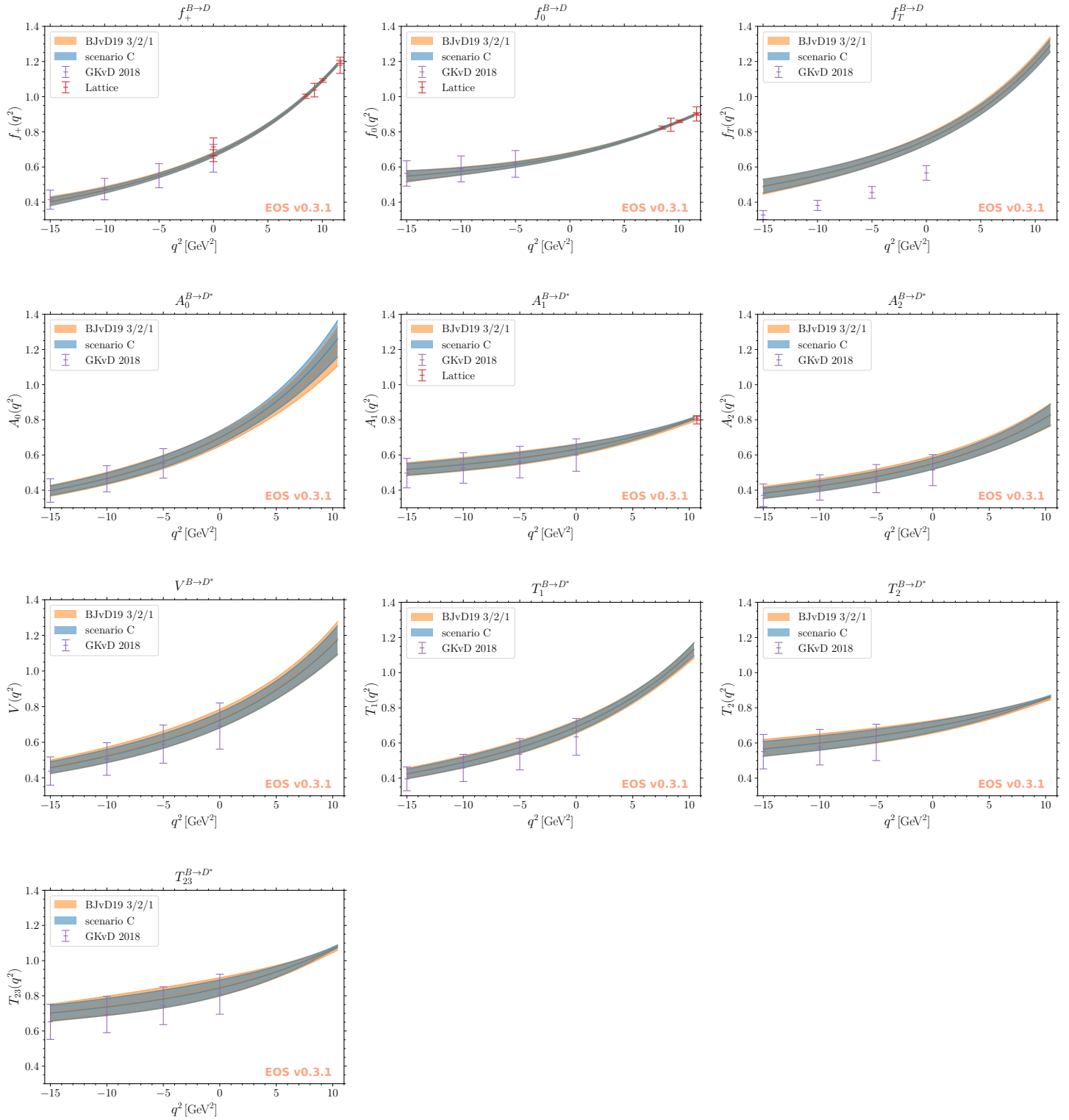


FIG. 1. The full set of $\bar{B} \rightarrow D^{(*)}$ form factors as a function of q^2 are used to showcase the agreement between the nominal results of ref. [19] (orange lines and areas) and the results when fully accounting for $\bar{B}_s^{(*)} \rightarrow D_s^{(*)}$ in the unitarity bounds (light blue lines and areas). For both sets of results we show the central values and 68% probability envelopes from posterior-predictive distributions of the respective fits. The LCSR results taken from ref. [26] (purple points) and lattice constraints (red points) used in the fits are also shown in the plots.

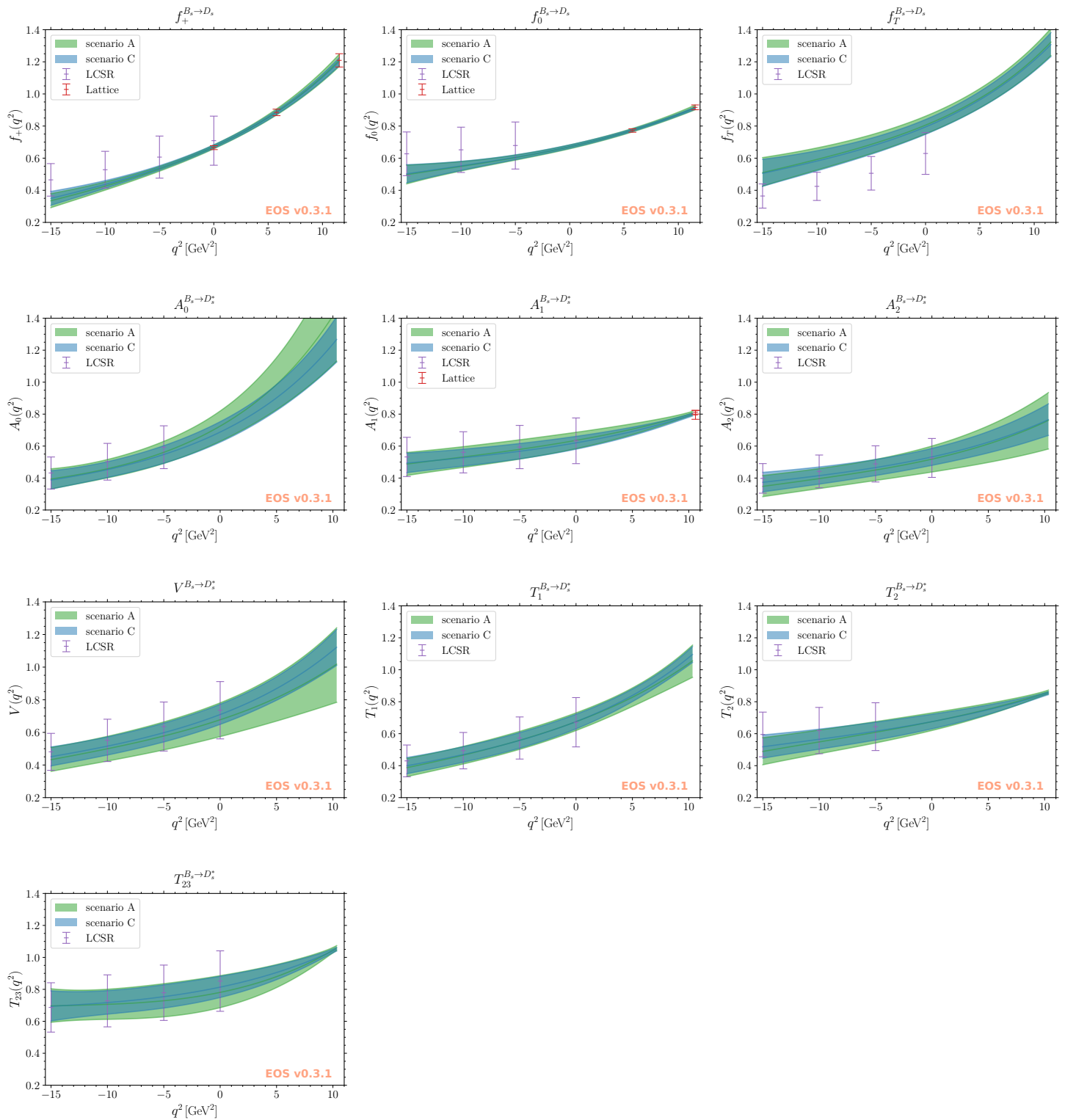


FIG. 2. Comparison between scenario A (green lines and areas) and scenario C (light blue lines and areas) of $\bar{B}_s \rightarrow D_s^{(*)}$ form factors as a function of q^2 . For both sets of results we show the central values and 68% probability envelopes from posterior-predictive distributions of the respective fits. The LCSR (purple points, see appendix B) and lattice QCD constraints used in the fits (red points, see refs. [34–37]) are also shown in the plots.

we provide the 17 independent coefficients up to order z^2 separately for the \bar{B} and \bar{B}_s decays. We exclude $a_0^{A_5}$, which can be obtained as

$$\frac{a_0^{A_5}}{a_0^{A_1}} = 2\sqrt{2}\frac{1-\sqrt{r}}{1+\sqrt{r}}, \quad (5)$$

where $r = m_{D_q^*}/m_{\bar{B}_q}$. Both sets of coefficients are provided exclusively within scenario C, for the two fits to either the nominal theory likelihood, or to the combined theory and experimental likelihood.¹

Effects on the unitarity bounds The question that started this analysis is regarding the saturation of the unitarity bounds when forgoing the assumption of $SU(3)_F$ symmetry. We find the best-fit points of ref. [19] to fully saturate the bounds of that analysis, as does the best-fit point of our scenario C in this analysis. This can be understood, since the bounds represent a non-linear prior on the HQE parameter space, and the likelihoods exhibit their global minimum outside of the support of this prior. The bounds can therefore be saturated to 100%, which poses another question: How likely is any given level of saturation of the bounds? This question can best be answered by computing the posterior predictive distributions of the contributions to the unitarity bounds. These distributions yield the probability density of each bound within the model description, given the available data. In figure 3, we juxtapose the results obtained for the $3/2/1$ model in ref. [19] with our results in scenario C. We find that the mode, *i.e.*, the most likely level of saturation, in both the 0^+ and the 0^- bounds increases from ~ 0.4 to ~ 0.6 . At the amplitude level this represents a relative increase of 22%. Including the results for $q = s$ spectators in the bounds therefore increases the average saturation of the bounds, and yields further and significant restrictions on the HQE parameter space. The prevailing assumption of *reducing* the $q = s$ contributions to the unitarity bounds by 20% should therefore be abandoned for future analyses. We obtain the following median values and central 68% intervals are for the four channels:

$$\begin{aligned} (J^P = 0^+) & \quad \text{median} = 0.62, \quad 68\% \text{ interval} : [0.37, 0.85], \\ (J^P = 0^-) & \quad \text{median} = 0.65, \quad 68\% \text{ interval} : [0.43, 0.88], \\ (J^P = 1^+) & \quad \text{median} = 0.08, \quad 68\% \text{ interval} : [0.05, 0.11], \\ (J^P = 1^-) & \quad \text{median} = 0.09, \quad 68\% \text{ interval} : [0.05, 0.11]. \end{aligned} \quad (6)$$

With this result, we illustrate that the unitarity bounds for the scalar and pseudoscalar currents have now become an indispensable ingredient in fitting any data on the form factors within the HQE. We note in passing that we find no significant shifts in the saturation of the bounds when using the combined theoretical and experimental likelihood.

Predictions for the lepton-flavour universality (LFU) ratios With the posterior samples of the various fits in hand, we can proceed to produce posterior predictive distributions for the LFU ratios.

Within the fit of scenario A to the likelihood comprised only of theory predictions of $\bar{B}_s \rightarrow D_s^{(*)}$ matrix elements, we obtain for the median values and central 68% probability intervals:

$$R(D_s) = 0.2979 \pm 0.0044, \quad R(D_s^*) = 0.246 \pm 0.010, \quad (7)$$

with negligible correlation between both results.

Within the fit of scenario C to the nominal theory-only likelihood, we obtain the following as the median values and central 68% probability intervals of all four LFU ratios:

$$\begin{aligned} R(D) &= 0.2989 \pm 0.0032, \quad R(D_s) = 0.2970 \pm 0.0034, \\ R(D^*) &= 0.2472 \pm 0.0050, \quad R(D_s^*) = 0.2450 \pm 0.0082. \end{aligned} \quad (8)$$

In this way, we obtain central values of the theory prediction of $R(D_s)$ and $R(D_s^*)$ which are lower than the results in scenario A by 0.7%. At the same time, we reduce the uncertainty of these predictions by 25–30%. The predictions for $R(D)$ and $R(D^*)$ stay virtually the same when compared to the theory-only results of ref. [19], with shifts smaller

¹ Note that these values do not obey the equation of motion $f_0(q^2 = 0) = f_+(q^2 = 0)$ exactly. If desired, one of the BGL coefficients in this relation can be replaced by the remaining ones in order to enforce this identity. The correlation matrix for the joined set of $\bar{B}_q \rightarrow D_q^{(*)}$ form factors becomes non-trivial due to additional relations between the BGL coefficient to the order in $1/m_{c,b}$ we are working in. This matrix can be obtained on request.

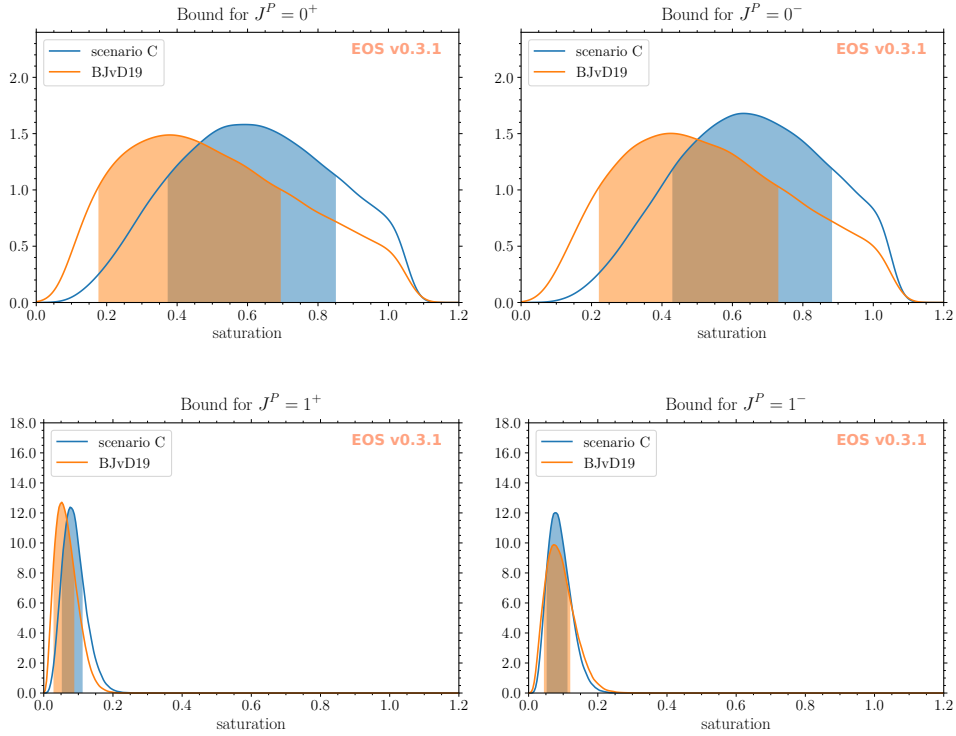


FIG. 3. Posterior predictive distributions for the unitarity bounds in the channels $J^P = 0^+, 0^-, 1^+, \text{ and } 1^-$. We compare the results from this work (blue lines and shaded areas) with the results obtained in ref. [19] (orange lines and shaded areas).

than 0.4% and only a small reduction in the uncertainty of $R(D^*)$. The correlation matrix for our theory predictions is:

$$\begin{pmatrix} 1.0000 & 0.1257 & 0.1294 & -0.0205 \\ 0.1257 & 1.0000 & 0.0031 & 0.3826 \\ 0.1294 & 0.0031 & 1.0000 & 0.0016 \\ -0.0205 & 0.3826 & 0.0016 & 1.0000 \end{pmatrix}, \quad (9)$$

in the order $R(D)$, $R(D^*)$, $R(D_s)$, and $R(D_s^*)$. Generally, the strongest correlations arise between the states with equal spin, since identical combinations of IW functions enter. However, since potential correlations in the lattice QCD data for $\bar{B} \rightarrow D$ and $\bar{B}_s \rightarrow D_s$ are unknown, the resulting correlations are smaller between these modes. The correlation between $R(D)$ and $R(D^*)$ results mainly from the LCSR results; the corresponding one for \bar{B}_s decays is much smaller and therefore so is the final correlation between $R(D_s)$ and $R(D_s^*)$.

When using the combined theoretical and experimental likelihood, we obtain in the same way as above:

$$\begin{aligned} R(D) &= 0.2981 \pm 0.0029, & R(D_s) &= 0.2971 \pm 0.0034, \\ R(D^*) &= 0.2504 \pm 0.0026, & R(D_s^*) &= 0.2472 \pm 0.0077. \end{aligned} \quad (10)$$

The correlation matrix now reads:

$$\begin{pmatrix} 1.0000 & 0.0855 & 0.1293 & -0.0504 \\ 0.0855 & 1.0000 & -0.0132 & 0.1768 \\ 0.1293 & -0.0132 & 1.0000 & 0.0036 \\ -0.0504 & 0.1768 & 0.0036 & 1.0000 \end{pmatrix}. \quad (11)$$

Polarizations in $\bar{B}_q \rightarrow D_q^{(*)} \tau^- \bar{\nu}$ We produce posterior predictive distributions for the τ polarization $P_\tau^{D_q^{(*)}}$ in $\bar{B}_q \rightarrow D_q^{(*)} \tau^- \bar{\nu}$ decays and the longitudinal polarization fraction F_L in $\bar{B}_q \rightarrow D_q^* \tau^- \bar{\nu}$ decays. In scenario C, using

model	scenarios			
	3/2/1	3/2/1	scenario C	scenario C
exp. likelihood	—	all exp.	—	all exp.
$\mathcal{B}(\bar{B}^0 \rightarrow D^+ \{e^-, \mu^-\} \bar{\nu})/ V_{cb} ^2$	13.48 ± 0.37	13.56 ± 0.35	13.48 ± 0.34	13.54 ± 0.32
$\mathcal{B}(\bar{B}^0 \rightarrow D^{*+} \{e^-, \mu^-\} \bar{\nu})/ V_{cb} ^2$	33.16 ± 2.15	32.00 ± 1.03	33.87 ± 1.82	32.69 ± 0.76
correlation	0.14	0.10	0.13	0.09
$ V_{cb} \times 10^3$ from $\bar{B} \rightarrow D \{e^-, \mu^-\} \bar{\nu}$	40.7 ± 1.2	40.6 ± 1.1	40.7 ± 1.1	40.7 ± 1.1
$ V_{cb} \times 10^3$ from $\bar{B} \rightarrow D^* \{e^-, \mu^-\} \bar{\nu}$	39.3 ± 1.7	40.0 ± 1.1	38.8 ± 1.4	39.5 ± 0.9
$ V_{cb} \times 10^3$ combined incl. corr.	40.2 ± 1.0	40.3 ± 0.8	40.0 ± 0.9	40.0 ± 0.7
$\mathcal{B}(\bar{B}_s^0 \rightarrow D_s^+ \{e^-, \mu^-\} \bar{\nu})/ V_{cb} ^2$	—	—	14.00 ± 0.40	13.99 ± 0.40
$\mathcal{B}(\bar{B}_s^0 \rightarrow D_s^{*+} \{e^-, \mu^-\} \bar{\nu})/ V_{cb} ^2$	—	—	33.04 ± 2.88	32.06 ± 2.54
correlation	—	—	-0.07	-0.10

TABLE III. Branching ratios and $|V_{cb}|$ predictions from [19] and scenario C in this work, with and without experimental data.

only theory constraints, we obtain

$$\begin{aligned}
P_\tau^D &= 0.3212 \pm 0.0029, & -P_\tau^{D^*} &= 0.484 \pm 0.017, \\
& & F_L &= 0.473 \pm 0.011, \\
P_\tau^{D_s} &= 0.3226 \pm 0.0096, & -P_\tau^{D_s^*} &= 0.477 \pm 0.025, \\
& & F_L^s &= 0.478 \pm 0.018.
\end{aligned} \tag{12}$$

Once we include the experimental PDFs in scenario C, we obtain

$$\begin{aligned}
P_\tau^D &= 0.3209 \pm 0.0029, & -P_\tau^{D^*} &= 0.492 \pm 0.013, \\
& & F_L &= 0.467 \pm 0.009, \\
P_\tau^{D_s} &= 0.3233 \pm 0.0095, & -P_\tau^{D_s^*} &= 0.486 \pm 0.023, \\
& & F_L^s &= 0.471 \pm 0.016.
\end{aligned} \tag{13}$$

Angular observables Using the theory only fit within scenario C we predict the angular observables J_i that arise in the four-fold differential decay rate of $\bar{B}_q \rightarrow D_q^* \{\mu^-, \tau^-\} \bar{\nu}$ decays, see *e.g.* ref. [39]. Our results are presented using the same convention as in ref. [40]. The central values with uncertainties are listed in table IV while the correlation matrices are given as ancillary files attached to the arXiv preprint of this article. While there are presently no measurements of the full set of these observables, an analysis strategy was recently suggested that allows to extract them without model bias at the Belle II and LHCb experiments [41].

Impact on $|V_{cb}|$ We find reasonable agreement between the values of $|V_{cb}|$ extracted in ref. [19] and in our analysis. When extracting from $\bar{B} \rightarrow D \ell^- \bar{\nu}$, $|V_{cb}|$ remains entirely stable. When extracting $|V_{cb}|$ from $\bar{B} \rightarrow D^* \ell^- \bar{\nu}$, we observe a small downward shift in the simultaneous analysis to the theory-only likelihood, which is almost entirely compensated when fitting to the combined likelihood. We find that the compatibility with the inclusive determination worsens slightly to 1.8σ from the previous result of 1.2σ . We average the exclusive and inclusive determinations, and obtain

$$|V_{cb}| = (41.1 \pm 0.5) \cdot 10^{-3},$$

which has smaller uncertainties than any of the previous determinations.

IV. SUMMARY AND OUTLOOK

We present the first simultaneous analysis of the form factors in $\bar{B}_q \rightarrow D_q^{(*)} \ell^- \bar{\nu}$ decays with $q = u, d, s$ beyond the $SU(3)_F$ symmetry limit. In addition to all available lattice QCD data our analysis makes use of two new sets of results, which have been produced for this work. First, we include new light-cone sum rule (LCSR) results for all

transition observable	$\bar{B} \rightarrow D^* \mu^- \bar{\nu}$	$\bar{B} \rightarrow D^* \tau^- \bar{\nu}$	$\bar{B}_s \rightarrow D_s^* \mu^- \bar{\nu}$	$\bar{B}_s \rightarrow D_s^* \tau^- \bar{\nu}$
J_1^s	0.257 ± 0.007	0.279 ± 0.006	0.255 ± 0.012	0.277 ± 0.009
J_2^c	-0.399 ± 0.008	-0.128 ± 0.001	-0.402 ± 0.015	-0.127 ± 0.002
J_2^s	0.085 ± 0.002	0.047 ± 0.001	0.085 ± 0.004	0.047 ± 0.002
J_3	-0.133 ± 0.004	-0.082 ± 0.002	-0.135 ± 0.006	-0.082 ± 0.003
J_4	-0.230 ± 0.001	-0.105 ± 0.001	-0.231 ± 0.003	-0.105 ± 0.002
J_5	0.167 ± 0.008	0.207 ± 0.005	0.161 ± 0.012	0.204 ± 0.007
J_6^c	0.011 ± 0.001	0.277 ± 0.015	0.011 ± 0.001	0.282 ± 0.023
J_6^s	-0.203 ± 0.012	-0.163 ± 0.012	-0.194 ± 0.016	-0.155 ± 0.015

TABLE IV. Central values and uncertainties for the non-redundant and non-vanishing angular observables in $\bar{B}_q \rightarrow D_q^* \{\mu^-, \tau^-\} \bar{\nu}$ in the Standard Model.

$\bar{B}_s \rightarrow D_s^{(*)} \ell^- \bar{\nu}$ form factors except $f_T^{(s)}$, which are obtained close to and beyond the point of maximum recoil. Second, we revisit the existing QCD sum rules for the subleading Isgur-Wise (IW) functions. We obtain a consistent set of predictions for both light and strange spectator quarks. Our results for the light spectator are consistent with previous numerical results in the literature [8]. A clear benefit of our simultaneous analysis is that we are no longer forced to make assumption about the $q = s$ form factors in the unitarity bounds.

We consider three different fit scenarios, all of which fit our various datasets well. Scenario A is used only when fitting exclusively the form factors for $q = s$ spectator quarks, and shows compatibility with $SU(3)_F$ symmetry in a first test. Scenarios B and C are used in simultaneous fits to both $q = u, d$ and $q = s$ data. Scenario C is more constrained, since it assumes a combined power counting in which $1/m_c$ power corrections in the HQE are of similar size as the $SU(3)_F$ breaking. Through a Bayesian model comparison, we find that scenario C is the most efficient in describing the available data, and we therefore only use this scenario to obtain all nominal results of our analysis. Using 34 parameters, scenario C can predict a total of 20 form factors in the entire semileptonic phase space. We make this information available through ancillary files, both for the parametrization in terms of parameters of the IW functions as well as those in the BGL parametrization. Our results include furthermore precise SM predictions for the branching ratios, lepton-flavour universality ratios, the complete non-redundant and non-vanishing set of angular observables in $\bar{B}_q \rightarrow D_q^* \{\mu^-, \tau^-\} \bar{\nu}$ decays, and the tau polarizations. We find good agreement between our results and the results of ref. [19], indicated by sub-percent shifts in the predictions of q^2 integrated observables. The precision of our predictions for observables in semileptonic $\bar{B}_s \rightarrow D_s^{(*)}$ decays has now reached a similar level as the prediction for observables in semileptonic $\bar{B}_{u,d} \rightarrow D_{u,d}^{(*)}$ decays.

To obtain a better understanding of the structure of the unitarity bounds, we analyze posterior predictive distributions of the saturation of the bounds. We find that our simultaneous analysis increases the median saturation compared to the previous analysis by $\sim 22\%$ at the amplitude level, which is of the same order as the naive reduction based on simple dimensional estimates of the $SU(3)_F$ breaking used in previous applications of the unitarity bounds. This reflects the observation that the form factors are perfectly compatible with $SU(3)_F$ symmetry at the present level of precision. Combining the $q = u, d$ and $q = s$ likelihoods in a simultaneous fit shows clear benefits: first, the unitarity bounds yield stronger constraints on the parameters space due to the larger degree of saturation. Second, the parametric uncertainties for all the IW functions decrease, with the largest effects in the parameters of the subsubleading IW functions. The consequence of both effects is a significant increase in the precision of the theory predictions of all observables considered in this work. Moreover, our analysis will be able to serve as an important cross check of the upcoming lattice QCD results for $\bar{B}_q \rightarrow D_q^*$ form factors, which can subsequently be included in order to be used in the analysis of future measurements in these decays.

Note added: In January 2020, the LHCb collaboration made public a first determination of $|V_{cb}|$ from $\bar{B}_s \rightarrow D_s^{(*)} \mu^- \bar{\nu}$ decays [42]. Unfortunately, this analysis does not include the required information to repeat this determination within our framework. However, we can determine the compatibility of the LHCb results for the quark flavour ratios R and

parameter	value	unit	reference
$\langle 0 \bar{q}q 0\rangle(2\text{ GeV})$	$-(0.272 \pm 0.010)^3$	GeV^3	[37, 43, 44]
$R_{\bar{q}q} \equiv \langle 0 \bar{s}s 0\rangle/\langle 0 \bar{q}q 0\rangle$	1.05 ± 0.20	—	[43–45]
$\langle 0 \frac{\alpha_s}{\pi}GG 0\rangle$	0.012 ± 0.012	GeV^4	[46–50]
m_0^2	0.8 ± 0.2	GeV^2	[51]
$R_{\bar{q}Gq} \equiv \langle 0 \bar{s}\sigma Gs 0\rangle/\langle 0 \bar{q}\sigma Gq 0\rangle$	0.85 ± 0.10	—	[52, 53]

TABLE V. Central values and uncertainties used in the QCDSR analysis.

subleading IW	value
$\hat{\eta}(1)$	$+0.71 [+0.49, +0.93]$
$\hat{\eta}'(1)$	$-0.06 [-0.40, +0.28]$
$\hat{\chi}_2(1)$	$-0.06 [-0.10, -0.02]$
$\hat{\chi}'_2(1)$	$-0.01 [-0.05, +0.03]$
$\hat{\chi}'_3(1)$	$+0.04 [+0.00, +0.08]$
$\hat{\eta}^{(s)}(1)$	$+0.75 [+0.49, +1.01]$
$\hat{\eta}^{(s)'}(1)$	$-0.05 [-0.40, +0.32]$
$\hat{\chi}_2^{(s)}(1)$	$-0.07 [-0.11, -0.03]$
$\hat{\chi}_2^{(s)'}(1)$	$+0.00 [-0.04, +0.04]$
$\hat{\chi}_3^{(s)'}(1)$	$-0.01 [+0.03, +0.07]$

TABLE VI. Numerical results for the subleading IW functions estimated by QCD sum-rules for both $q = u, d$ and $q = s$ cases.

R^* ,

$$R^{(*)} \equiv \frac{\mathcal{B}(\bar{B}_s \rightarrow D_s^{(*)} \mu^- \bar{\nu})}{\mathcal{B}(\bar{B} \rightarrow D^{(*)} \mu^- \bar{\nu})}, \quad (14)$$

with our theory predictions. We obtain $R = 1.038 \pm 0.034$ and $R^* = 0.975 \pm 0.076$ with a correlation of -2.58% . Our results are compatible with the LHCb results at 0.1σ . Additionally, LHCb has published the ratio of the D_s^* branching ratio over the D_s branching ratio in the semimuonic decay. Our result for this ratio, 0.424 ± 0.040 is compatible with the LHCb result at 0.7σ .

ACKNOWLEDGMENTS

We thank Donal Hill for helpful discussions on the prospects of measuring the angular observables at LHCb. We are grateful to Christoph Bobeth for pointing out a typo in the manuscript.

The work of MB is supported by the Deutsche Forschungsgemeinschaft (DFG, German Research Foundation) under grant 396021762 - TRR 257. The work of MJ is supported by the Italian Ministry of Research (MIUR) under grant PRIN 20172LNEEZ. The work of NG and DvD is supported by the DFG within the Emmy Noether Programme under grant DY130/1-1 and the DFG Collaborative Research Center 110 ‘‘Symmetries and the Emergence of Structure in QCD’’. We thank the DFG Excellence Cluster ‘‘Origins and Structure of the Universe’’ for supporting a short-term visit of MB.

Appendix A: QCD Three-Point Sum Rule Results: Inputs and Results

We evaluate the existing three-point QCD sum rule calculations for the subleading IW functions of refs. [23–25] for $q = s$ and, in order to remain consistent within our analysis, also for $q = u, d$. This generalization is possible since potential unknown perturbative or power corrections $\sim m_s$ are suppressed additionally at least by $\alpha_s \varepsilon_c$ and included in our treatment of the uncertainties. The sum rules depend on perturbative parameters (α_s, μ), parameters pertaining only to the sum rules (Borel parameters, threshold parameters), and non-perturbative inputs (QCD condensates). The value for α_s is chosen consistent with the rest of our calculation, and the sum-rule specific parameters are chosen

parameter	value	unit	reference
$\bar{m}_c(\bar{m}_c)$	1.28 ± 0.03	GeV	as in [26]
f_{B_s}	0.2307 ± 0.0013	GeV	[55]
f_{D_s}	0.2499 ± 0.0004	GeV	[55]
$f_{D_s^*}$	0.293 ± 0.019	GeV	[56]
M^2	4.5 ± 1.5	GeV ²	[57]

TABLE VII. The central values and prior ranges for the the charm quark mass, the decay constants and the Borel parameter used to estimate the LCSRs for the $\bar{B}_s \rightarrow D_s^{(*)}$ form factors.

within the ranges of the original calculations. The values for the condensates are listed in table V. A couple of comments are in order:

- We increase the uncertainty for the light-quark condensate in order to ensure consistency with the values obtained in the calculations used for the strange-quark condensate.
- The gluon condensate remains very difficult to calculate in general, and existing lattice calculations yield also large ranges. We use the “traditional” value [46, 47], but increase its uncertainty to account for other results in the literature, for instance [48–50].²
- The parameter m_0^2 for the mixed quark-gluon condensate is defined via $\langle 0|\bar{q}\sigma Gq|0\rangle \equiv m_0^2\langle 0|\bar{q}q|0\rangle$; its $SU(3)$ -breaking seems to be under control [52, 53].

The $SU(3)$ -breaking parameters are of the expected order; the subleading IW functions for $\bar{B}_s^{(*)} \rightarrow D_s^{(*)}$ are consequently compatible with the non-strange ones. We reproduce the central values previously obtained in refs. [8, 23–25] for $q = u, d$ when using their input values. In refs. [8, 25] the uncertainties for $\eta^{(\prime)}(1)$ have been approximately doubled compared to the parametric ones, in order to account for the uncertainties inherent to the method. We follow the same recipe for the other parameters as well. We obtain the final central values and uncertainties the following way: we consider each sum rule separately, varying the sum-rule specific parameters freely within their ranges (corresponding to the R-fit treatment [54]), while assuming Gaussian uncertainties for the condensates. We symmetrize the obtained interval for $\Delta\chi^2 = 1$ and then double the corresponding uncertainty. We do not include the resulting sizable correlations between the IW parameters, which we consider to be a conservative approach. We checked that the value obtained for $\xi^{(s)'}(1)$ from the sum rule for the leading IW function (which is not used as a separate theory input) is compatible with the value obtained in our fits. This is not true for the second derivative, which, however, does not enter the results for the parameters of the subleading IW functions up to the first derivative; hence we do not consider the sum-rule results for the second derivatives. Our results are summarized in table VI.

Appendix B: Light-Cone Sum Rule: Inputs and Results

To obtain numerical results for the $\bar{B}_s \rightarrow D_s^{(*)}$ form factors (FFs) at and above maximum hadronic recoil, we employ the QCD sum rules on the light cone (LCSRs) with B -meson distribution amplitudes (LCDAs) [57]. An advantageous feature of LCSRs is that the analytical form of the results depends only on the Dirac structure of the correlator used to compute them and on universal hadronic input in form of the LCDAs, but not on the quark flavour. We can employ the results derived in ref. [26] for the $B \rightarrow \{P, V\}$ transitions to compute the $\bar{B}_s \rightarrow D_s^{(*)}$ form factors to twist-four accuracy and at leading order in α_s .

The parameters that enter the LCSRs are:

- the charm quark mass $\bar{m}_c(\bar{m}_c)$ in the $\overline{\text{MS}}$ scheme;
- the decay constants f_{B_s} and $f_{D_s^{(*)}}$ of the respective meson states;
- the B_s -to-vacuum matrix elements of local $\bar{s}Gb$ currents $\lambda_{B_s, E}^2, \lambda_{B_s^*, E}^2$;

² Note that a different definition is also common in the literature, without the factor of π in the denominator.

- the inverse moment of the B_s light-cone distribution amplitude $1/\lambda_{B_s,+}$;
- the Borel parameter M^2 ;
- the duality thresholds $s_0^{(F)}$, where F enumerate all of the $\bar{B}_s \rightarrow D_s^{(*)}$ form factors.

The central values and prior ranges for the charm quark mass, the decay constants and the Borel parameter are compiled in table VII together with their respective sources. The values used for the $\bar{s}Gb$ matrix elements and the inverse moment of the B_s light-cone distribution amplitude require some comments: The $\bar{s}Gb$ matrix elements provide the normalization of the three-parton LCDAs. Their contributions to the form factors is small compared to the numerically leading two-parton terms [26]. Consequently, potential $SU(3)_F$ symmetry-breaking effects are not relevant here, and we use the strict $SU(3)_F$ limit [58]:

$$\lambda_{B_s,E}^2 = \lambda_{B_d,E}^2 = 0.03 \pm 0.02, \quad \lambda_{B_s,H}^2 = \lambda_{B_d,H}^2 = 0.06 \pm 0.03. \quad (\text{B1})$$

On the other hand, the inverse moment $1/\lambda_{B_s,+}$ of the leading-twist B_s LCDA ϕ_+ requires a more detailed discussion, due to its bigger impact on the numerical results. To leading order in α_s and within the exponential model used here, the following relation holds[59]:

$$\lambda_{B_q,+} = \frac{2}{3} \bar{\Lambda}_q. \quad (\text{B2})$$

However, this relation is known to be subject to UV-divergent corrections in fixed-order perturbation theory [60]. We therefore suggest to estimate the difference of $\lambda_{B_d,+}$ and $\lambda_{B_s,+}$ in which these UV-divergent terms cancel in the $SU(3)_F$ limit. Using $SU(3)_F$ symmetry for the power-suppressed term $\lambda_1 = -0.30 \text{ GeV}^2$, the forward matrix element of the kinetic operator, we obtain $\bar{\Lambda}_d = 0.500 \text{ GeV}$ and $\bar{\Lambda}_s = 0.590 \text{ GeV}$. To be consistent with the previous LCSR analysis of the $\bar{B} \rightarrow D^{(*)}$ form factors [26] we use $\lambda_{B_d,+} = 0.460 \pm 0.110 \text{ GeV}$ [61], and estimate:

$$\lambda_{B_s,+} = \lambda_{B_d,+} + \frac{2}{3} (\bar{\Lambda}_s - \bar{\Lambda}_d) = 0.520 \pm 0.110 \text{ GeV}. \quad (\text{B3})$$

For our analysis we adopt the same Borel parameters as for the $\bar{B} \rightarrow D^{(*)}$ analysis carried out in ref [26]. We also ensure that

1. under variation of the Borel parameters M^2 in the chosen intervals the sum rule yields stable results;
2. the contributions due to continuum and excited states above the respective thresholds $s_0^{(F)}$ are small compared to the ground state contribution, i.e., the integral from $s = 0$ to $s_0^{(F)}$;
3. contributions at higher twists remain small.

The variation of our sum rules in the Borel windows given in table VII contributes 9% to the overall systematic uncertainty of our results, which is larger than what was obtained for the $\bar{B} \rightarrow D^{(*)}$ analysis [26]. We further account for the absence of $1/m_b^2$ in the correlator by assigning an additional 5% to the systematic uncertainty. Adding the two in quadrature yields an overall systematic uncertainty of $\sim 10\%$.

The thresholds $s_0^{(F)}$ are determined using the same procedure as proposed in ref. [62] and subsequently employed in ref. [26]. The basic idea is to take the derivative of the FF sum rule with respect to $-1/M^2$ and to normalize the derivative to the FF sum rule itself, obtaining (schematically) the squared meson mass-estimator

$$[M_{D^{(*)}}^2]_{\text{LCSR}} = \frac{\int_0^{s_0^{(F)}} e^{-\frac{s}{M^2}} s \rho_F(s, q^2)}{\int_0^{s_0^{(F)}} e^{-\frac{s}{M^2}} \rho_F(s, q^2)}, \quad (\text{B4})$$

with ρ_F standing in for the spectral density from which we extract the form factor F . Following [26], we impose 5% uncertainties on the estimator of the squared meson mass, to account for higher twist correction to the spectral density $\rho_F(s, q^2)$. We also vary q^2 from -15 GeV^2 to 0 GeV^2 , for which we find that q^2 dependence of the estimator $[M^2]_{\text{LCSR}}$ is negligible. We use $s_0^{(F)}(q^2) \equiv s_0^{(F)}$. The union of the threshold intervals at 68% probability for each of the FFs³ reads:

$$s_0^{(F)} = [6.9, 11.0] \text{ GeV}^2 \quad \text{for } \bar{B}_s \rightarrow D_s, \quad (\text{B5})$$

$$s_0^{(F)} = [7.9, 11.8] \text{ GeV}^2 \quad \text{for } \bar{B}_s \rightarrow D_s^*. \quad (\text{B6})$$

³ Except for $f_T^{B \rightarrow D}$, for which the threshold determination has not been possible for the same reasons illustrated in [26]. We follow the same procedure as outlined there to estimate the f_T threshold parameter using the f_+ threshold parameter.

Our predictions for the full set of form factors and for the set excluding f_T , both evaluated at $q^2 = \{-15, -10, -5, 0\}$ GeV² and including the covariance matrix across form factors and across q^2 points, are published as part of the EOS software [27] as of version v0.3.1. Both sets of predictions can be accessed as multivariate Gaussian constraints named

```
B_s->D_s^(*)::FormFactors[f_+,f_0,f_T,A_0,A_1,A_2,V,T_1,T_2,T_23]@BGJvD2019,
B_s->D_s^(*)::FormFactors[f_+,f_0,A_0,A_1,A_2,V,T_1,T_2,T_23]@BGJvD2019,
```

respectively. In addition, we provide these predictions as machine readable ancillary files attached to this preprint.

-
- [1] W. Altmannshofer *et al.* (Belle-II), (2018), arXiv:1808.10567 [hep-ex].
- [2] A. Cerri *et al.*, CERN Yellow Rep. Monogr. **7**, 867 (2019), arXiv:1812.07638 [hep-ph].
- [3] R. Aaij *et al.* (LHCb), Eur. Phys. J. **C73**, 2373 (2013), arXiv:1208.3355 [hep-ex].
- [4] Y. S. Amhis *et al.* (HFLAV), (2019), arXiv:1909.12524 [hep-ex].
- [5] R. Glattauer *et al.* (Belle), Phys. Rev. **D93**, 032006 (2016), arXiv:1510.03657 [hep-ex].
- [6] A. Abdesselam *et al.* (Belle), (2017), arXiv:1702.01521 [hep-ex].
- [7] A. Abdesselam *et al.* (Belle), (2018), arXiv:1809.03290 [hep-ex].
- [8] F. U. Bernlochner, Z. Ligeti, M. Papucci, and D. J. Robinson, Phys. Rev. **D95**, 115008 (2017), [erratum: Phys. Rev. **D97**, no. 5, 059902 (2018)], arXiv:1703.05330 [hep-ph].
- [9] D. Bigi and P. Gambino, Phys. Rev. **D94**, 094008 (2016), arXiv:1606.08030 [hep-ph].
- [10] D. Bigi, P. Gambino, and S. Schacht, JHEP **11**, 061 (2017), arXiv:1707.09509 [hep-ph].
- [11] D. Bigi, P. Gambino, and S. Schacht, Phys. Lett. **B769**, 441 (2017), arXiv:1703.06124 [hep-ph].
- [12] B. Grinstein and A. Kobach, Phys. Lett. **B771**, 359 (2017), arXiv:1703.08170 [hep-ph].
- [13] F. U. Bernlochner, Z. Ligeti, M. Papucci, and D. J. Robinson, Phys. Rev. **D96**, 091503 (2017), arXiv:1708.07134 [hep-ph].
- [14] S. Jaiswal, S. Nandi, and S. K. Patra, JHEP **12**, 060 (2017), arXiv:1707.09977 [hep-ph].
- [15] M. Jung and D. M. Straub, JHEP **01**, 009 (2019), arXiv:1801.01112 [hep-ph].
- [16] P. Gambino, M. Jung, and S. Schacht, Phys. Lett. **B795**, 386 (2019), arXiv:1905.08209 [hep-ph].
- [17] T. D. Cohen, H. Lamm, and R. F. Lebed, Phys. Rev. **D100**, 094503 (2019), arXiv:1909.10691 [hep-ph].
- [18] N. Das and R. Dutta, (2019), arXiv:1912.06811 [hep-ph].
- [19] M. Bordone, M. Jung, and D. van Dyk, (2019), arXiv:1908.09398 [hep-ph].
- [20] I. Caprini, L. Lellouch, and M. Neubert, Nucl. Phys. **B530**, 153 (1998), arXiv:hep-ph/9712417 [hep-ph].
- [21] N. Isgur and M. B. Wise, Phys. Lett. **B232**, 113 (1989).
- [22] N. Isgur and M. B. Wise, *DPF Conf.1990:0459-464*, Phys. Lett. **B237**, 527 (1990).
- [23] M. Neubert, Z. Ligeti, and Y. Nir, Phys. Lett. **B301**, 101 (1993), arXiv:hep-ph/9209271 [hep-ph].
- [24] M. Neubert, Z. Ligeti, and Y. Nir, Phys. Rev. **D47**, 5060 (1993), arXiv:hep-ph/9212266 [hep-ph].
- [25] Z. Ligeti, Y. Nir, and M. Neubert, Phys. Rev. **D49**, 1302 (1994), arXiv:hep-ph/9305304 [hep-ph].
- [26] N. Gubernari, A. Kokulu, and D. van Dyk, JHEP **01**, 150 (2019), arXiv:1811.00983 [hep-ph].
- [27] D. van Dyk *et al.*, “EOS — A HEP program for Flavor Observables,” (2019), version 0.3.1, available from <https://eos.github.io>, doi:10.5281/zenodo.3569692.
- [28] E. McLean, C. T. H. Davies, J. Koponen, and A. T. Lytle, (2019), arXiv:1906.00701 [hep-lat].
- [29] M. Atoui, V. Morénas, D. Bećirevic, and F. Sanfilippo, Eur. Phys. J. **C74**, 2861 (2014), arXiv:1310.5238 [hep-lat].
- [30] J. A. Bailey *et al.*, Phys. Rev. **D85**, 114502 (2012), [Erratum: Phys. Rev. **D86**, 039904 (2012)], arXiv:1202.6346 [hep-lat].
- [31] J. A. Bailey *et al.* (MILC), Phys. Rev. **D92**, 034506 (2015), arXiv:1503.07237 [hep-lat].
- [32] E. McLean, C. T. H. Davies, A. T. Lytle, and J. Koponen, Phys. Rev. **D99**, 114512 (2019), arXiv:1904.02046 [hep-lat].
- [33] H. Jeffreys, *The Theory of Probability*, 3rd ed. (Oxford University Press, 1998).
- [34] J. A. Bailey *et al.* (Fermilab Lattice, MILC), Phys. Rev. **D89**, 114504 (2014), arXiv:1403.0635 [hep-lat].
- [35] H. Na, C. M. Bouchard, G. P. Lepage, C. Monahan, and J. Shigemitsu (HPQCD), Phys. Rev. **D92**, 054510 (2015), [Erratum: Phys. Rev. **D93**, no. 11, 119906 (2016)], arXiv:1505.03925 [hep-lat].
- [36] J. Harrison, C. Davies, and M. Wingate (HPQCD), Phys. Rev. **D97**, 054502 (2018), arXiv:1711.11013 [hep-lat].
- [37] S. Aoki *et al.* (Flavour Lattice Averaging Group), (2019), arXiv:1902.08191 [hep-lat].
- [38] C. G. Boyd, B. Grinstein, and R. F. Lebed, Phys. Lett. **B353**, 306 (1995), arXiv:hep-ph/9504235 [hep-ph].
- [39] M. Duraisamy, P. Sharma, and A. Datta, Phys. Rev. **D90**, 074013 (2014), arXiv:1405.3719 [hep-ph].
- [40] T. Feldmann, B. Müller, and D. van Dyk, Phys. Rev. **D92**, 034013 (2015), arXiv:1503.09063 [hep-ph].
- [41] D. Hill, M. John, W. Ke, and A. Poluektov, JHEP **11**, 133 (2019), arXiv:1908.04643 [hep-ph].
- [42] R. Aaij *et al.* (LHCb), (2020), arXiv:2001.03225 [hep-ex].
- [43] C. McNeile, A. Bazavov, C. T. H. Davies, R. J. Dowdall, K. Hornbostel, G. P. Lepage, and H. D. Trottier, Phys. Rev. **D87**, 034503 (2013), arXiv:1211.6577 [hep-lat].
- [44] C. T. H. Davies, K. Hornbostel, J. Komijani, J. Koponen, G. P. Lepage, A. T. Lytle, and C. McNeile (HPQCD), Phys. Rev. **D100**, 034506 (2019), arXiv:1811.04305 [hep-lat].
- [45] L. J. Reinders, H. Rubinstein, and S. Yazaki, Phys. Rept. **127**, 1 (1985).
- [46] M. A. Shifman, A. I. Vainshtein, and V. I. Zakharov, Nucl. Phys. **B147**, 385 (1979).
- [47] M. A. Shifman, A. I. Vainshtein, and V. I. Zakharov, Nucl. Phys. **B147**, 448 (1979).

- [48] B. L. Ioffe, Phys. Atom. Nucl. **66**, 30 (2003), [Yad. Fiz.66,32(2003)], arXiv:hep-ph/0207191 [hep-ph].
- [49] R. Horsley, G. Hotzel, E. M. Ilgenfritz, R. Millo, H. Perlt, P. E. L. Rakow, Y. Nakamura, G. Schierholz, and A. Schiller, Phys. Rev. **D86**, 054502 (2012), arXiv:1205.1659 [hep-lat].
- [50] G. S. Bali, C. Bauer, and A. Pineda, Phys. Rev. Lett. **113**, 092001 (2014), arXiv:1403.6477 [hep-ph].
- [51] V. M. Belyaev and B. L. Ioffe, Sov. Phys. JETP **56**, 493 (1982), [Zh. Eksp. Teor. Fiz.83,876(1982)].
- [52] M. Beneke and H. G. Dosch, Phys. Lett. **B284**, 116 (1992).
- [53] V. M. Braun and A. Lenz, Phys. Rev. **D70**, 074020 (2004), arXiv:hep-ph/0407282 [hep-ph].
- [54] A. Hocker, H. Lacker, S. Laplace, and F. Le Diberder, Eur. Phys. J. **C21**, 225 (2001), arXiv:hep-ph/0104062 [hep-ph].
- [55] A. Bazavov *et al.*, Phys. Rev. **D98**, 074512 (2018), arXiv:1712.09262 [hep-lat].
- [56] P. Gelhausen, A. Khodjamirian, A. A. Pivovarov, and D. Rosenthal, Phys. Rev. **D88**, 014015 (2013), [Erratum: Phys. Rev. **D91**,099901(2015)], arXiv:1305.5432 [hep-ph].
- [57] S. Faller, A. Khodjamirian, C. Klein, and T. Mannel, Eur. Phys. J. **C60**, 603 (2009), arXiv:0809.0222 [hep-ph].
- [58] T. Nishikawa and K. Tanaka, Nucl. Phys. **B879**, 110 (2014), arXiv:1109.6786 [hep-ph].
- [59] A. G. Grozin and M. Neubert, Phys. Rev. **D55**, 272 (1997), arXiv:hep-ph/9607366 [hep-ph].
- [60] S. J. Lee and M. Neubert, Phys. Rev. **D72**, 094028 (2005), arXiv:hep-ph/0509350 [hep-ph].
- [61] V. M. Braun, D. Yu. Ivanov, and G. P. Korchemsky, Phys. Rev. **D69**, 034014 (2004), arXiv:hep-ph/0309330 [hep-ph].
- [62] I. Sentitemsu Imsong, A. Khodjamirian, T. Mannel, and D. van Dyk, JHEP **02**, 126 (2015), arXiv:1409.7816 [hep-ph].